Isotopic variation of dissolved and colloidal iron and copper in a carbonatic floodplain soil after experimental flooding

Charirat Kusonwiriyawong[a], Moritz Bigalke[a*], Florian Abgottspon[a], Marina Lazarov[b], Stephan Schuth[b], Stefan Weyer[b], Wolfgang Wilcke[c]

[a]Geographic Institute, University of Berne, Hallerstrasse 12, 3012 Berne, Switzerland

[b]Institute of Mineralogie, Leibniz University Hannover, Callinstrasse 3
30167 Hannover, Germany

[c]Institute of Geography and Geoecology, Karlsruhe Institute of Technology (KIT), Reinhard-Baumeister-Platz 1, 76131 Karlsruhe, Germany.

[*]Corresponding author: Moritz Bigalke, phone: +41(0)316314055, moritz.bigalke@giub.unibe.ch

Abstract

Many floodplain soils worldwide are contaminated by present and past industrial and mining activities. During flooding redox potential decreases, triggering the release of dissolved and colloidal metals. We used an anaerobic microcosm incubation to simulate flooding of a carbonate-rich floodplain soil for 40 days. Soil solution samples were extracted to determine the release of dissolved (<0.02 µm) and colloidal fractions (0.02 - 10 µm). We analyzed stable isotope ratios of colloidal and dissolved Fe and Cu representing two groups of metals with different release behavior; release of Fe was steadily increasing, while Cu peaked sharply after flooding and decreased afterwards. The temporal trend of δ^{56}Fe values of total Fe in

solution indicated dissimilatory iron reduction. The apparent isotopic fractionation between dissolved and colloidal Fe ($\Delta^{56}Fe_{dissolved\text{-}colloidal} = \delta^{56}Fe_{dissolved} - \delta^{56}Fe_{colloidal}$) varied between 0.31±0.04‰ and -1.86±0.26‰. Low $\delta^{56}Fe_{colloidal}$ (-1.16±0.04 ‰) values on day 4 of the experiment suggested colloid formation by precipitation of dissolved Fe, while the strong temporal variation in $\Delta^{56}Fe_{dissolved\text{-}colloidal}$ indicated subsequent changes in colloid mineralogy, sorption to soil components and/or electron transfer-atom exchange. The variations in $\delta^{65}Cu$ values ($\Delta^{65}Cu_{dissolved\text{-}colloidal}$ from 0.81±0.03‰ to 1.58±0.09‰) are probably linked to changing oxidation state of colloidal Cu. While at the beginning of the experiment colloidal Cu and solid soil Cu exchange, these systems decouple after the onset of sulfate reduction in the second half of the experiment. The experimental results fit well to findings from redoximorphic soils described in the literature and highlight the importance of colloids for metal release and the isotopic pattern in carbonatic soils.

Keywords: Copper, Iron, Soil, Redox Processes, Colloids, Stable Metal Isotopes

Highlights

- Colloidal Fe precipitates from dissolved Fe in soil solution and does not originate from the mobilization of solid Fe minerals.
- The $\delta^{56}Fe$ value of colloidal Fe changes with time indicating changes in mineralogy or electron transfer-atom exchange.
- Colloidal and solid soil Cu exchange occurs until sulfate reduction starts, afterwards colloidal Cu decouples from solid soil and colloids aggregate.
- The $\Delta^{65}Cu_{dissolved\text{-}colloidal}$ values are probably driven by the redox state of colloidal Cu.
- Experimental findings agree well with field observations.

47

48 **Graphical Abstract**

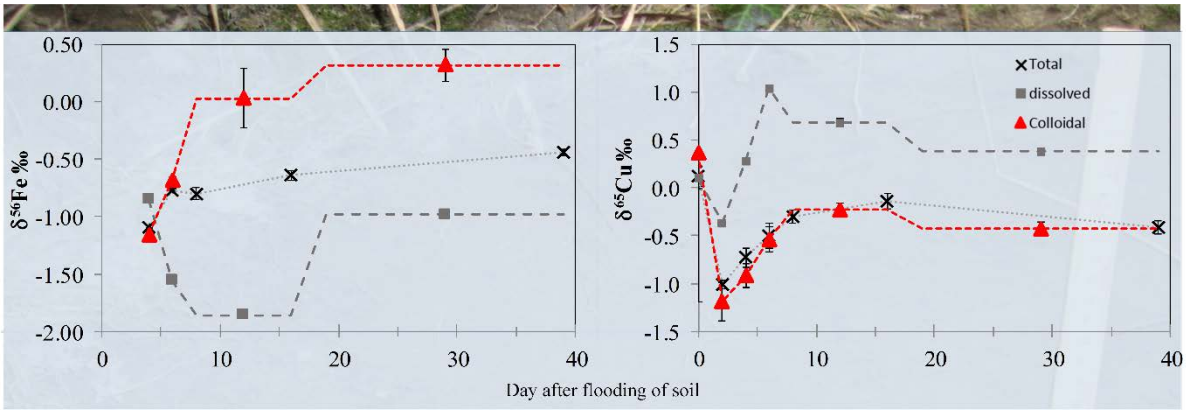

49

50

1. Introduction

Present and past industrial and mining activities release contaminants into rivers, which continuously accumulate in floodplain soils (Burton et al., 2008; Frohne et al., 2011; Hindersmann and Mansfeldt, 2014). Depending on the frequency of flooding, metals might be remobilized and contaminate ground and surface waters (Du Laing et al., 2007; Hindersmann et al., 2014; Mansfeldt and Overesch, 2013). The mobility of metals mainly depends on organic matter concentrations and composition, soil mineral composition, redox conditions, and carbonate concentrations (Du Laing et al., 2009). When soils are flooded, the redox potential (E_h) decreases and Fe and Mn (oxyhydr)oxides are dissolved in many soils releasing associated trace elements (e.g., As, Ba, Co, Cr, V; Abgottspon et al., 2015; Hindersmann and Mansfeldt, 2014; Weber et al., 2009b). In some soils with permanent water saturation, the pool of reducible Fe and Mn is depleted and no further mobilization occurs under anoxic conditions. The release kinetics depends strongly on crystallinity of Fe and Mn minerals and microbial community composition in the soil (Lovley, 1991; Schuth et al., 2015). In carbonatic soils, the pH is buffered by the carbonic acid-hydrogen carbonate buffer system and proton release during formation of minerals like siderite and rhodochrosite (Abgottspon et al., 2015; Ponnamperuma, 1972). Furthermore, changes to anoxic conditions may cause microbial formation of reduced metal colloids (e.g., Cu^0, Weber et al., 2009b). When E_h decreases, microbial sulfate reduction may be initialized and mobility of metals can be limited by the formation of or co-precipitation with sulfides (Borch et al., 2010; Weber et al., 2009a). However, sulfate reduction may also favor the release of metal-sulfide colloids of some elements (e.g., Ag, Cd, Cu, Hg, Pb) resulting in enhanced metal mobility during several days after flooding (Abgottspon et al., 2015; Hofacker et al., 2013; Weber et al., 2009b). The formation of sulfides is limited by the available sulfate content and controlled by the solubility of the corresponding metal sulfides (Weber et al., 2009a). Beside the formation of

organic, biomineralized and sulfide colloids, also colloids of Fe and Mn minerals may favor trace element transport (Hassellov and von der Kammer, 2008). The colloids may form because of precipitation of siderite and rhodochrosite in carbonatic soils or the precipitation of mixed valence (oxyhydr)oxides (e.g., magnetite or green rust; Ratering and Schnell, 2000; Tadanier et al., 2005; Taylor, 1980). Another colloid formation process is the partial reduction of ferrihydrite by microorganisms which may initialize deflocculation and release of the remaining ferrihydrite as colloids along with associated non-Fe elements (Tadanier et al., 2005). When soil flooding ends and redox conditions change back from anoxic to oxic, sulfides will be oxidized, releasing metals like Cd, Cu and Zn to pore waters, which may (co)precipitate with (oxyhydr)oxides (Contin et al., 2007; Du Laing et al., 2007; Frohne et al., 2011).

Abgottspon et al. (2015) differentiated trace metals into two groups with different release behavior in water-saturated soils. When E_h decreased (from 300 mV to 0 mV), Group I metals (Ba, Co, Cr, Ni, and V) were constantly released during 40 days, predominantly in dissolved form (<50 % as colloids) closely correlated with the release of Fe and Mn by reductive dissolution of (oxyhydr)oxides. The increase in colloidal concentrations of Group I metals is probably attributable to coprecipitation of dissolved metals with and sorption to colloidal Fe and Mn minerals. Group II metals (Ag, Cd, Cu and Pb) were rapidly released after 2-6 days of flooding, strongly dominated by the colloidal fraction (>80%; 0.02-10 µm). In this study, we focus on the stable isotope ratios of Fe and Cu as representatives of Group I and Group II metals, respectively, to further explore the mechanisms underlying the observed differences in the release behavior of the two metal groups.

The stable isotope ratios of Fe and Cu bear a high potential to investigate long-term biogeochemical processes in soils, especially redox processes (Babcsanyi et al., 2014; Bigalke et al., 2013; Bigalke et al., 2010b; Mansfeldt et al., 2012; Wiederhold et al., 2007a). Iron is an important driver of biogeochemical processes and trace metal behavior in soils. Changing the

oxidation state of Fe results in marked Fe isotope fractionation causing variations in Fe isotopic composition among Fe pools in anoxic soils with $\delta^{56}Fe$ values ranging from -5‰ to +1‰ (Johnson et al., 2008). Under anoxic conditions, dissimilatory iron reduction (DIR) by bacteria initializes three main Fe reaction pools, i.e. $Fe^{2+}_{(aq)}$, $Fe^{2+}_{(sorb)}$ and $Fe^{3+}_{(reac)}$. Some of the dissolved $Fe^{2+}_{(aq)}$ may sorb to the oxide surface as $Fe^{2+}_{(sorb)}$. Electron transfer between $Fe^{2+}_{(sorb)}$ and Fe^{3+} creates a reactive layer of Fe^{3+} at the oxide surface ($Fe^{3+}_{(reac)}$) and is associated with ^{56}Fe enrichment in the solid phase. Subsequently, DIR releases isotopically light Fe into solution while heavy Fe isotopes are preferentially adsorbed on Fe oxide surfaces ($\Delta^{56}Fe_{mineral\text{-}solution}$ up to 4‰; Frierdich et al., 2014; Icopini et al., 2004; Mikutta et al., 2009; Teutsch et al., 2005). The apparent isotope fractionation between $Fe^{2+}_{(aq)}$ and $Fe^{3+}_{(reac)}$ is identical regardless of bacteria species or type of oxides yielding $\Delta^{56}Fe_{Fe(II)\text{-}Fe(III)reac}$ values of ~ -3‰ (Crosby et al., 2007). When the reduction continues, increased Fe^{2+} concentrations in solution result in a shift to a heavier Fe isotopic composition of dissolved Fe because of isotopic pool-size effects. This fractionation depends on the relative proportion of the three main reactive Fe pools (Crosby et al., 2007). Schuth et al. (2015) conducted incubation experiments under controlled E_h conditions and found strong variations in bulk $\delta^{56}Fe$ values in soil solutions of a surface soil horizon, while a permanently anoxic lower soil horizon showed no Fe release and no response of $\delta^{56}Fe$ values to flooding, probably because of a more stable crystalline Fe oxide mineralogy or an absence of Fe-reducing bacteria. However, at constant E_h a steady state of $\delta^{56}Fe$ values and dissolved total Fe was observed by Schuth et al. (2015) for the topsoil because of the balance of Fe release and removal from solution. Garnier at al. (2017) and Thompson et al. (2007) found Rayleigh-type fractionation during DIR in redox-influenced soils but smaller fractionation compared to the experimentally determined fractionation factors, because of additional processes occurring in soil (e.g. organic complexation).

Ilina et al. (2013a) studied iron isotope variations in river, lake and mire waters and soil solutions of different filtration sizes reaching from 100 µm to <1 kDa. The $\delta^{57}Fe$ values of mire waters (0.12 to 0.66 ‰) and soil solutions (-0.20 to -0.42 ‰) showed no systematic differences except for the <1 kDa fraction, which was the lightest (-0.83 to -0.91 ‰). River waters became constantly heavier (up to 4.2 ‰) with decreasing pore size, which was explained by stronger Fe binding of low molecular weight organic compounds compared to bigger particles like Fe (oxyhydr)oxides (Ilina et al., 2013a). A similar observation was made by Schuth and Mansfeldt (2016) for stagnant water, where smaller particles indicated a slight enrichment in ^{56}Fe. Furthermore, other mechanisms can induce Fe isotope fractionation. Heavy Fe isotopes are preferentially adsorbed or precipitated on the bacterial cell surface ($\Delta^{56}Fe_{cell\text{-}solution}$ up to 1.7‰) and complexed by organic ligands ($\Delta^{56}Fe_{complex\text{-}solution}$ of 0.6‰; Brantley et al., 2001; Dideriksen et al., 2008; Morgan et al., 2010; Mulholland et al., 2015). Precipitation of siderite caused a lighter Fe isotope ratio in the siderite ($\Delta^{56}Fe_{dissolved\text{-}siderite}$ = 0.0-0.9‰; Johnson et al., 2005; Wiesli et al., 2004). While kinetic FeS precipitation caused an enrichment of light Fe in the precipitate ($\Delta^{56}Fe_{Fe(II)aq\text{-}FeS}$ = 0.85±0.30‰; Butler et al., 2005), precipitation of mackinawite at equilibrium conditions caused oppositional fractionation of $\Delta^{56}Fe_{Fe(II)aq\text{-}mackinawite}$ = -0.32±0.29‰ to -0.64±0.36‰ (Guilbaud et al., 2011; Wu et al., 2011). The precipitation of magnetite similarly causes an enrichment of heavy isotopes in the precipitates ($\Delta^{56}Fe_{Fe(II)aq\text{-}magnetite}$ = -1.34±0.11‰ to -1.56±0.20‰; Frierdich et al., 2014; Johnson et al., 2005).

Sorption of Cu to Al and Fe (oxyhydr)oxides causes an enrichment of heavy Cu on the surface of these minerals with $\Delta^{65}Cu_{solid\text{-}solution}$ values of up to 1‰ (Balistrieri et al., 2008; Pokrovsky et al., 2008). Sorption to organic ligands shows varying fractionation with $\Delta^{65}Cu_{solid\text{-}solution}$ values between -0.3 and 0.8‰ depending on type of organic ligand and pH (Bigalke et al., 2010a; Navarette et al., 2011; Ryan et al., 2014). Lighter Cu isotopes are preferentially adsorbed on clay mineral surfaces with $\Delta^{65}Cu_{adsorbed\text{-}solution}$ values of -0.3‰ (Li

et al., 2015). Copper uptake into bacteria also causes various Cu isotope fractionations depending on organism and pH. Mainly the lighter Cu isotope is preferentially incorporated into the live bacteria cell ($\Delta^{65}Cu_{bacteria\text{-}solution}$ = 0 to -4.4 ‰; Navarette et al., 2011; Pokrovsky et al., 2008; Zhu et al., 2002). In redox reactions, the reduced Cu species is enriched in lighter Cu isotopes (e.g., $\Delta^{65}Cu_{solution\text{-}covellite}$ = 3.06‰; Ehrlich et al., 2004 and $\Delta^{65}Cu_{Cu2+\text{-}CuI}$ = 4 ‰; Zhu et al., 2002). Bigalke et al. (2010b, 2011, 2013) found episodically water-saturated soil to be enriched in heavy Cu isotopes, which they attributed to the loss of light Cu by leaching of reduced colloidal Cu forms. Ilina et al. (2013b) found no significant variations (δ^{65}Cu values of 0.36 to 0.46 ‰) between differently filtered fractions (100µm - <1kDa) of river water, which they attributed to similar bonding strength of Cu fulvic complexes of different mass. Vance et al. (2008) reported lighter δ^{65}Cu values (-0.24 to -1.02‰) in the particulate fraction of rivers compared to the dissolved phase (0.42 to 0.94‰) and explained this with strong bonding of dissolved Cu to organic complexes.

In this study, we investigate the isotope geochemistry of dissolved and colloidal Fe and Cu in a water-saturated carbonatic soil. Our goals are to better understand how a) Fe (oxyhydr)oxide dissolution and Fe colloid formation and b) Cu release and colloid formation in soils affect isotopic composition of soils and soil solutions. We furthermore will link our experimental results to field observations previously reported in the literature.

2. Materials and methods

A Calcaric Fluvisol (IUSS, 2014), with high calcium carbonate content (420 g kg^{-1}) was sampled near the city of Aesch in Switzerland (47°28'39" N / 7°36'21" E). The soil had a neutral pH (7.4), an organic carbon concentration of 21.7 g kg^{-1}, a total Fe concentration of 12.6 g kg^{-1} and a dithionite-extractable Fe concentration of 7.87 g kg^{-1} (Abgottspon et al., 2015). More details about the soil are given in Table S1. The soil was located next to the river Birs on a floodplain with temporary flooding (Kayser et al., 2006). The sampling site was moderately contaminated with several trace metals (e.g.,

Cd, Cr, Cu, Pb, Table S1) by an adjacent non-ferrous metal smelter, causing elevated Cu concentrations of 122 mg kg^{-1} (Kusonwiriyawong et al., 2016). About 10 kg of topsoil were sampled from the Ah horizon (0-0.15 m depth) in March 2011. The soil was air-dried and sieved to <2 mm. The setup of the incubation experiment was similar to that of Weber et al. (2009b) and identical to that described in Abgottspon et al. (2015). In fact, samples were taken from exactly the same experiment described in Abgottspon et al. (2015). In summary, 1.7 L of artificial river water were filled in 3-L PE microcosms. The artificial river water (prepared from ultrapure water and clean salts) had a similar ionic strength and ionic composition as the river Birs next to the sampling site (0.92 mmol L^{-1} $CaCl_2$, 0.98 mmol L^{-1} $NaNO_3$, 0.84 mmol L^{-1} $MgSO_4$), but did not contain DOC, trace metals, or suspended matter. Then, 1.7 kg of air-dry soil was slowly added to the microcosm and stirred to ensure homogenization and removal of air bubbles, resulting in complete water saturation. After homogenization, the soil material was allowed to settle and around 2 cm of stagnant water covered the soil (Figure S1). Three replicate microcosms and one blank (i.e. only artificial river water) were set up in a glovebox (GS Glovebox Plexiglas, GS Glovebox Systemtechnik, Malsch, Germany) that was purged with nitrogen (Figure S2). The soil solution was extracted with PE suction cups with a 10-µm nominal pore size (ecoTech GmbH, Bonn, Germany) manually located in the lower half of the microcosms with a syringe. On each sampling date, 50 mL of solution was extracted. Over the whole experiment, we extracted 700 mL of a total solution volume of 1700 mL. Nevertheless, in the lower part of the microcosm the soil was always water-saturated (and the suction cup at this depth always flooded). Our extraction of solution might have simulated slow drainage as is also observed in natural soils. We realized mass balance calculations to check how repeated sampling of the microcosms may affect Fe and Cu concentrations and $\delta^{56}Fe$ and $\delta^{65}Cu$ values. Over the whole experiment we extracted 0.06% and 0.18% of the total Fe and Cu in the system, respectively. Taking the isotopic composition into account, the isotopic change of the total pool related to the sampling is insignificant (-0.001‰ and 0.002‰) for $\delta^{56}Fe$ and $\delta^{65}Cu$, respectively. These effects are much smaller than our analytical precision. Therefore, we conclude that the sampling will not significantly affect the isotopic composition of the total metal pools. The Eh and pH values were analysed directly after sampling in the glovebox. To rule out that the initial mobilization of colloids is an artifact caused by manually

sampling of the soil solution, Al concentrations were analyzed and found to be consistently low (on average 0.5 µmol L^{-1}). As Al is a major constituent of the soil (2.6 wt. %), low Al concentrations render the artificial release of soil colloids (e.g., clay minerals, Al hydroxides) unlikely. The solution is supposed to contain the total (colloidal + dissolved) element concentration (<10 µm). To determine dissolved element concentrations, samples were manually filtered to <0.02 µm using syringe filters (Anotop 25 Plus, Whatman, Bottingen, Switzerland) in the glove box directly after sampling. The Fe and Cu concentrations were analyzed by ICP-MS (7700x, Agilent, Santa Clara, California) using In and Rh as internal standards. The difference between total and dissolved elemental concentrations was assumed to be the colloidal fraction (0.02-10 µm). All unfiltered and filtered solutions were acidified with suprapur HNO_3 (ROTH, Karlsruhe, Germany) and stored at -20°C prior to isotope analysis. The Fe^{2+} concentration in the unfiltered solution was determined photometrically (Spectroquant Pharo 100, MERCK). Each 5-mL aliquot of unfiltered soil solution was treated with 50 µL of H_2SO_4 (25%, p.a.), 0.5 mL of ammonium-acetate-acetic acid (400 g L^{-1} ammonium acetate, 50% acetic acid) and 0.2 mL of phenanthrolin solution (5 g L^{-1} 1,10-phenanthroliumchlorid) and made up to 10 mL with Millipore water in the glovebox. Samples were measured after 15 minutes at the wavelength of 510 nm. A detailed evolution of E_h, pH, SO_4^{2-}, S^{2-}, Fe^{2+} C and metal concentrations in 2-4 day resolution is given in Tables S2 & S3 and Abgottspon et al. (2015).

For total digestion of the bulk soil sample, approximately 70 mg of soil was digested in HNO_3, HF and H_2O_2 (3:2:1) in PFA beakers (Savillex, MN, USA) at least 24 h on a hot plate at 120 °C. The digested samples were evaporated until dryness at 70 °C. Soil solution samples were evaporated in PFA vials (Savillex, MN, USA). The dried residues were digested using a mixture of concentrated HNO_3 and H_2O_2 (ratio 1:1) at 120°C for at least 3-4 hours and evaporated to dryness. The dried soil and solution samples were subsequently re-fluxed in HCl and HNO_3 (3:1) at least 3 h at 120 °C and finally dissolved in 7 mol L^{-1} HCl + 0.001% H_2O_2 for ion exchange separation. The total (<10µm) and dissolved (<0.02µm) fractions were analyzed in samples from Days 0, 2, 4, 6, 8, 11, 13, 16, 19, 22, 26, 30, 34 and 39. After 8 days of incubation, the dissolved Cu concentrations (<0.02µm) were too low to get the required

300 ng of Cu for the isotope analysis. Thus, samples from the dissolved fraction of days 8, 10, 13, and 16 were combined to a single composite sample and another composite sample was prepared from days 19, 22, 26, 30, 34 and 39. In these composite samples of the dissolved fraction, we also measured stable Fe isotope ratios after purification (see below). In addition, for Fe isotope measurement samples from the three replicates microcosms were combined to a composite sample of days 4 and 6, respectively, for both total (<10µm) and dissolved (<0.02µm) fractions because of too low mass (< 7µg Fe) of Fe for isotopic analysis at the beginning of the experiment. Copper and Fe fractions were purified as described in Bigalke et al. (2013). For solution samples, a single-step ion-exchange approach was sufficient to separate Cu and Fe from other matrix elements, while bulk soil samples were purified twice for Cu isotope analysis. All Fe and Cu fractions yielded an average recovery of 100.6±1.3% (mean±SD) and 101.1±2.1% (mean±SD), respectively. All samples which did not yield a recovery of within 100 ± 6% were discarded, and the purification process was repeated. The acids (HNO_3 and HCl) used in this study were purified by sub-boiling distillation in quartz stills or were purchased in suprapur quality. Other reagents were of suprapur quality. All solutions and dilute acids were prepared using 18 MΩ grade water (EMD Millipore, MA, USA). All sample preparations were performed in the clean chemistry laboratory at the Institute of Geology, University of Bern. The procedural blank was 3.1±1.8 ng (n=3) for Fe and 2.3±0.2 ng (n=3) for Cu, compared to at least 7000 and 300 ng of Fe and Cu, respectively, in the samples.

Iron and Cu isotope measurements were performed on a Thermo-Scientific Neptune Plus MC-ICP-MS at the Leibniz University Hannover, Germany. The Fe isotopic compositions were analyzed in the high mass resolution mode to resolve isobaric interferences of $^{40}Ar^{14}N^{+}$, $^{40}Ar^{16}O^{+}$, and $^{40}Ar^{16}OH^{+}$ on ^{54}Fe, ^{56}Fe, and ^{57}Fe (Weyer and Schwieters, 2003). Chromium (^{53}Cr) was monitored to correct isobaric interferences of ^{54}Cr on ^{54}Fe. The standard-sample bracketing method was applied in combination with external

element doping for mass bias correction. For the latter, the 5 mg L^{-1} Ni standard NIST 986 (National Institute of Standards and Technology, Gaithersburg, MA, USA) was doped to all Fe standards (IRMM-014, Institute for Reference Materials and Measurements, Geel, Belgium) and samples for mass-bias correction (Oeser et al., 2014). The Fe isotope standard (IRMM-014) and the samples were diluted to yield a concentration of 7 mg L^{-1} Fe with 2% HNO_3. Every sample was at least analyzed twice and the mean $\delta^{56}Fe$ value is given. The $\delta^{56}Fe$ values are reported relative to IRMM-014.

In a three-isotope plot, $\delta^{56}Fe$ and $\delta^{57}Fe$ values define a linear correlation (slope=1.4664, R^2= 0.99, Figure S3) following the theoretical mass-dependent fractionation line ($\delta^{57}Fe \sim 1.5 \times \delta^{56}Fe$) which indicates the absence of isobaric interferences (Malinovsky et al., 2003). The accuracy and precision of the Fe isotope analysis was monitored using an Fe-free matrix sample (BCR-2, Basalt Columbia River 2, USGS, Reston, VA, USA) that was doped with Fe of known isotopic composition, and an in-house standard (an Fe salt from ETH Zurich, Switzerland). The Fe-free matrix samples were prepared from the matrix fraction derived from the purification of the original samples which were doped with the Fe standard (Merck Certipur®, Darmstadt, Germany) and processed in the same way as the samples. The average $\delta^{56}Fe$ value of the matrix fraction was 0.19±0.03‰ (mean ±2SD, n=5) which is identical to the pure Merck Fe value (0.19±0.02‰, n=3). The USGS basalt BCR-2 yielded a mean $\delta^{56}Fe$ value of 0.07±0.02‰ (2SD, n=4) which agrees well with previously published values ranging from 0.05±0.02‰ to 0.11±0.03‰ (Craddock and Dauphas, 2011; Liu et al., 2014a; Schuth et al., 2015; Weyer et al., 2005). The average $\delta^{56}Fe$ value of our in-house standard was -0.69±0.02‰ (mean ± 2SD, n=6) and again in good agreement with previously published values varying from -0.71±0.18‰ to -0.73±0.10‰ (Fehr et al., 2008; Kiczka et al., 2011; Mansfeldt et al., 2012; Schuth et al., 2015).

For Cu isotope analysis, standard-sample bracketing was conducted in combination with external element doping for mass-bias correction. Again the Ni standard NIST 986 was

used for the mass-bias correction by analyzing $^{62}Ni/^{60}Ni$ (for details see Lazarov and Horn, 2015). The samples were diluted to yield a final concentration of 300 µg Cu L^{-1} and 1000 µg Ni L^{-1} and were measured with MC-ICP-MS in low resolution mode. Every sample was at least analyzed twice and the mean was reported. The $\delta^{65}Cu$ values are reported relative to the Cu standard NIST SRM 976 after external mass-bias correction using the exponential law. The success of the Cu purification and the accuracy and precision of the Cu isotope analysis was verified by using Cu-free matrix samples that were subsequently doped with Cu of known isotopic composition, and a basalt reference material (BCR-2). The Cu-free matrix samples were prepared from the matrix fraction derived from the purification of the original samples and doped with the ERM®-AE633 Cu isotope standards (Institute for Reference Materials and Measurements, Geel, Belgium), which is isotopically indistinguishable from NIST 976 (Moeller et al., 2012). The doped matrices were treated and purified in the same manner as the original samples. The average $\delta^{65}Cu$ value of the matrix samples was -0.02±0.01‰ (mean ± 2SD, n=3) which is identical to the value of ERM®-AE633 (-0.01±0.05‰; Moeller et al., 2012). The BCR-2 reference material yielded a mean of $\delta^{65}Cu_{NIST976}$ = 0.18±0.01‰ (2SD, n=3), which is in good agreement with previously published data ranging from 0.14±0.05‰ to 0.22±0.06‰ (Moeller et al., 2012). The external reproducibility was evaluated with the in-house Cu standard (NBS C 125-2) yielding an average $\delta^{65}Cu$ value of 0.37±0.06‰ (mean ±2SD, n=10).

Most isotopic compositions from our experiments are reported as means of the triplicate microcosm incubations (Table 1). Therefore, error bars in the figures do not reflect measurement uncertainties but variations among the triplicate microcosms reflecting the natural soil heterogeneity. The isotopic composition of the metal colloidal fraction (δ_{coll} = $\delta^{56}Fe$ and $\delta^{65}Cu$ values) was calculated from the difference in the isotopic composition of total and dissolved metal concentrations in solution based on isotopic mass balance, as show in Equation 1. To calculate colloidal concentrations and δ values of the composite samples,

313 we averaged the values of the colloidal concentrations and the δ values based on mass balance
314 approaches, as shown in Equation 2 with δ_{ss} and C_{ss} being the delta value and the
315 concentration of the respective subsample. In Equation 1-5 δ_{tot}, δ_{diss} and δ_{coll} are the $\delta^{56}Fe$ or
316 $\delta^{65}Cu$ and c_{tot}, c_{diss} and c_{coll} the concentrations of the total, dissolved and colloidal fraction,
317 while the prefix 2SD indicate the respective 2SD uncertainty.

318 $$\delta_{coll} = \frac{(\delta_{tot} \times [c_{tot}]) - (\delta_{diss} \times [c_{diss}])}{[c_{tot}] - [c_{diss}]} \quad (1)$$

319 $$\delta_{bulk} = \frac{\sum_{ss=1}^{s} \delta_{ss} \times [c_{ss}]}{\sum_{ss=1}^{s} [c_{ss}]} \quad (2)$$

320 The error of the δ value of the colloidal fraction calculated according to the general formula
321 of error propagation (Taylor, 1997) as shown in Equation 3.

322 $$2SD\delta_{coll} = \sqrt{\left(\frac{\partial \delta_{coll}}{\partial \delta_{tot}} 2SD\delta_{tot}\right)^2 + \left(\frac{\partial \delta_{coll}}{\partial c_{tot}} 2SDc_{tot}\right)^2 + \left(\frac{\partial \delta_{coll}}{\partial \delta_{diss}} 2SD\delta_{diss}\right)^2 + \left(\frac{\partial \delta_{coll}}{\partial c_{diss}} 2SDc_{diss}\right)^2}$$

323 (3)

324 If we apply Equation 3 to Equation 1, we get Equation 4, which allows calculating the
325 uncertainty of the δ values of the colloidal fraction as displayed in Table 1.

326 $$2SD\delta_{coll} = \sqrt{\left(\frac{c_{tot}}{c_{tot} - c_{diss}} 2SD\delta_{tot}\right)^2 + \left(-\frac{c_{diss}(\delta_{tot} - \delta_{diss})}{(c_{tot} - c_{diss})^2} 2SDc_{tot}\right)^2 + \left(-\frac{c_{diss}}{c_{tot} - c_{diss}} 2SD\delta_{diss}\right)^2 + \left(\frac{(\delta_{tot} - \delta_{diss})c_{tot}}{(c_{diss} - c_{tot})^2} 2SDc_{diss}\right)^2}$$

327 (4)

328 Finally, the error of the $\Delta_{dissolved\text{-}colloidal}$ values was calculated according to equation 5

329 $$2SD\Delta_{diss-coll} = \sqrt{(2SD\delta_{diss})^2 + (2SD\delta_{coll})^2} \quad (5)$$

Table 1 Concentration and isotopic compositions of Fe and Cu in bulk soil prior to flooding, total (<10µm), dissolved (<0.02 µm) and (calculated) colloidal (0.02-10 µm) fractions of soil solution during 40 days of experimental flooding.

Element	Bulk soil / day after flooding	Total					Dissolved					Colloidal			
		Conc. (µmol L^{-1})	SD	δ value (‰)	2SD	n[a]	Conc. (µmol L^{-1})	SD	δ value (‰)	2SD	n[a]	Conc.[h] (µmol L^{-1})	SD[e]	δ value[f] (‰)	2SD[g]
Fe	Soil	226000[b]	22920[b]	0.04	0.01	3	-	-	-	-	-	-	-	-	-
	4	41.4	2.86	-1.09	0.01	1	9.89	3.95	-0.85	0.01	1	31.6	4.88	-1.16	0.04
	6	116	0.24	-0.77	0.01	1	10.99	2.70	-1.56	0.01	1	105	2.71	-0.68	0.03
	8	181	7.36	-0.80	0.05	3	119[c]	19.8	-1.86[b]	0.03	1	197[c]	29.4	0.03	0.26
	16	452	25.6	-0.64	0.04	3									
	39	673	9.17	-0.44	0.03	3	394[d]	24.3	-0.98[c]	0.01	1	203[d]	25.9	0.32	0.14
Cu	Soil	1920[b]	70[b]	-0.08	0.04	3	-	-	-	-	-	-	-	-	-
	0	5.09	0.12	0.12	0.11	3	4.60	0.29	0.10	0.11	3	0.49	0.31	0.36	1.55
	2	23.0	1.59	-1.01	0.04	3	5.04	4.15	-0.37	0.04	3	18.0	4.45	-1.19	0.20
	4	20.4	2.30	-0.73	0.10	3	3.19	0.29	0.28	0.03	3	17.2	2.32	-0.92	0.12
	6	21.5	1.60	-0.50	0.13	3	0.53	0.23	1.04	0.03	1	21.0	1.62	-0.54	0.13
	8	14.4	1.46	-0.30	0.07	3	0.07[c]	0.03	0.68[c]	0.04	1	10.1	1.37	-0.23	0.07
	16	5.80	1.28	-0.14	0.08	3									
	39	2.64	0.82	-0.41	0.07	3	0.07[d]	0.02	0.38[d]	0.03	1	2.59	0.82	-0.43	0.07

[a]Number of replicate preparations and analysis, [b]Concentrations in the solid soil are in µmol kg^{-1}, [c]Bulked sample combined from days 8 to 16, [d]Bulked sample combined from days 19 to 39, [e]Calculated by error propagation of standard deviation in total and dissolved concentration, [f]Calculated by the difference between the δ^{65}Cu values of total and dissolved Cu (Eq. 1), [g]Calculated by error propagation according to Eq. S1-S4, [h]Calculated by substracting the dissolved from the total concentrations.

3. Results

Iron was first mainly released in colloidal form, which changed after 19 days to predominantly dissolved Fe (Figure 1 and Table S3, Abgottspon et al., 2015). On day 39, only 22% of the total Fe was still in colloidal form. The sum of total and dissolved Fe concentrations increased continuously until the end of the incubation, while the colloidal concentrations increased until day 16 and decreased afterwards (Figure 1). From day 2 on, the total Fe in solution was dominated by Fe^{2+}, but the concentration of Fe^{2+} started to deviate substantially from that of total Fe from day 13 on. After day 13, the Fe^{2+} concentrations showed only a slight increase until day 22 and a decrease afterwards. From day 22 on, the dissolved Fe concentration was even higher than that of total Fe^{2+} indicating that Fe^{3+} was also present in the dissolved phase. On day 29, only 33% of the total Fe in solution was still Fe^{2+}.

The Fe isotope composition of total Fe in solution started at negative $\delta^{56}Fe$ values on day 4 and afterwards increased slightly (Figure 2b). The $\delta^{56}Fe$ value of total Fe in solution was correlated with the total Fe concentrations in solution (Figure 3). The $\delta^{56}Fe$ value of the colloidal Fe sharply increased on day 6 and then gradually continued to increase until the end of incubation, and was parallel to the evolution of the $\delta^{56}Fe$ values of the total Fe in solution (Figure 2b). The $\delta^{56}Fe$ values of the dissolved fraction were higher than the colloidal fraction on day 4. Then, $\delta^{56}Fe$ values of the dissolved fraction continuously decreased from day 4 to day 8-16. After 19-39 days, the $\delta^{56}Fe$ values of dissolved Fe shifted to heavier values (Figure 2b). The $\Delta^{56}Fe_{dissolved\text{-}colloidal}$ value decreased from 0.31±0.04‰ on day 4 to -1.86±0.26‰ on day 12 and thereafter increased slightly (Figure 4a). The $\delta^{56}Fe$ value of the bulk soil was 0.04±0.01‰ (n=3).

Copper was also mainly released in colloidal form but in contrast to Fe, Cu release peaked around day 6 and decreased thereafter (Figure 2c, Abgottspon et al., 2015). The $\delta^{65}Cu$ values of the total, dissolved and colloidal Cu fractions did not differ from each other and

were close to that of the bulk soil at the start of the experiment (day 0; Figure 2d). With strongly increasing Cu concentrations in solution on day 2, the $\delta^{65}Cu$ value of total Cu in solution shifted to lower values and later on back towards initial values (Figure 2d). The $\delta^{65}Cu$ value in both colloidal and dissolved Cu decreased markedly on day 2. After day 2, the $\delta^{65}Cu$ value of the colloidal Cu increased until day 16; thereafter the $\delta^{65}Cu$ value decreased slightly until the end of the experiment. The $\delta^{65}Cu$ value of the dissolved fraction increased as well until day 6, but then, decreased towards the end of the experiment. The $\Delta^{65}Cu_{dissolved-colloidal}$ value changed from a maximum of 1.58±0.13‰ on day 6 back to 0.81±0.03‰ at the end of the experiment (Figure 4b). The $\Delta^{65}Cu_{dissolved-colloidal}$ from day 0 of the experiment could not be used because of the high uncertainty of the $\delta^{65}Cu_{coll}$ value at this day (Tab. 1). The $\delta^{65}Cu$ value of the bulk soil was -0.08±0.04‰ (n=3).

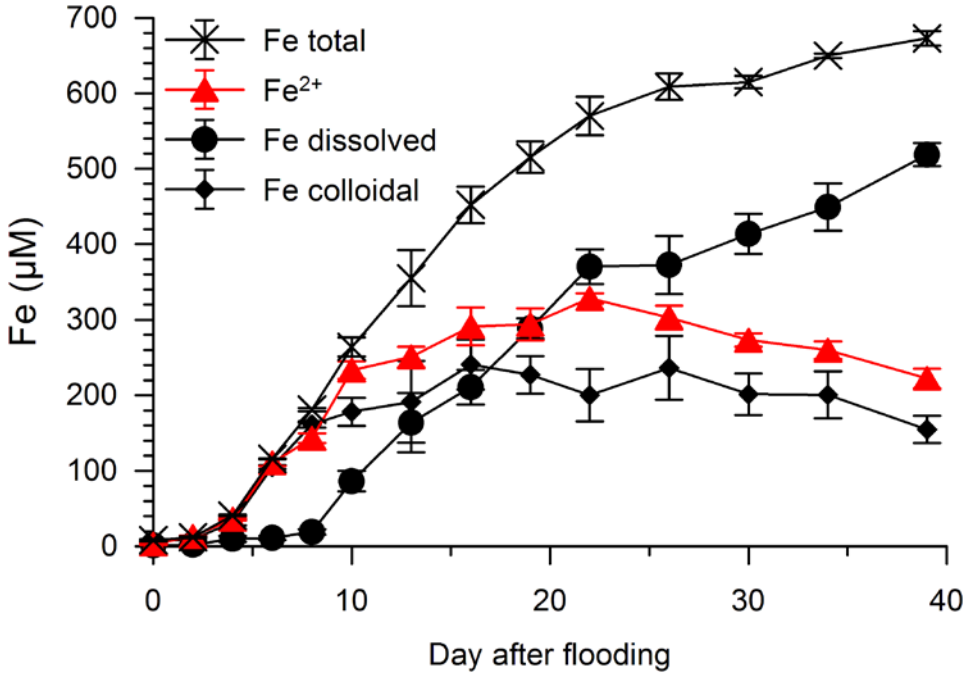

Figure 1 Fe concentrations in total, dissolved and colloidal Fe during the experiment. Total, dissolved and colloidal Fe concentrations were taken from Abgottspon et al. (2015). The Fe^{2+} concentrations were specifically measured for this study in unfiltered samples and therefore represent total Fe^{2+} in solution including dissolved an colloidal fractions.

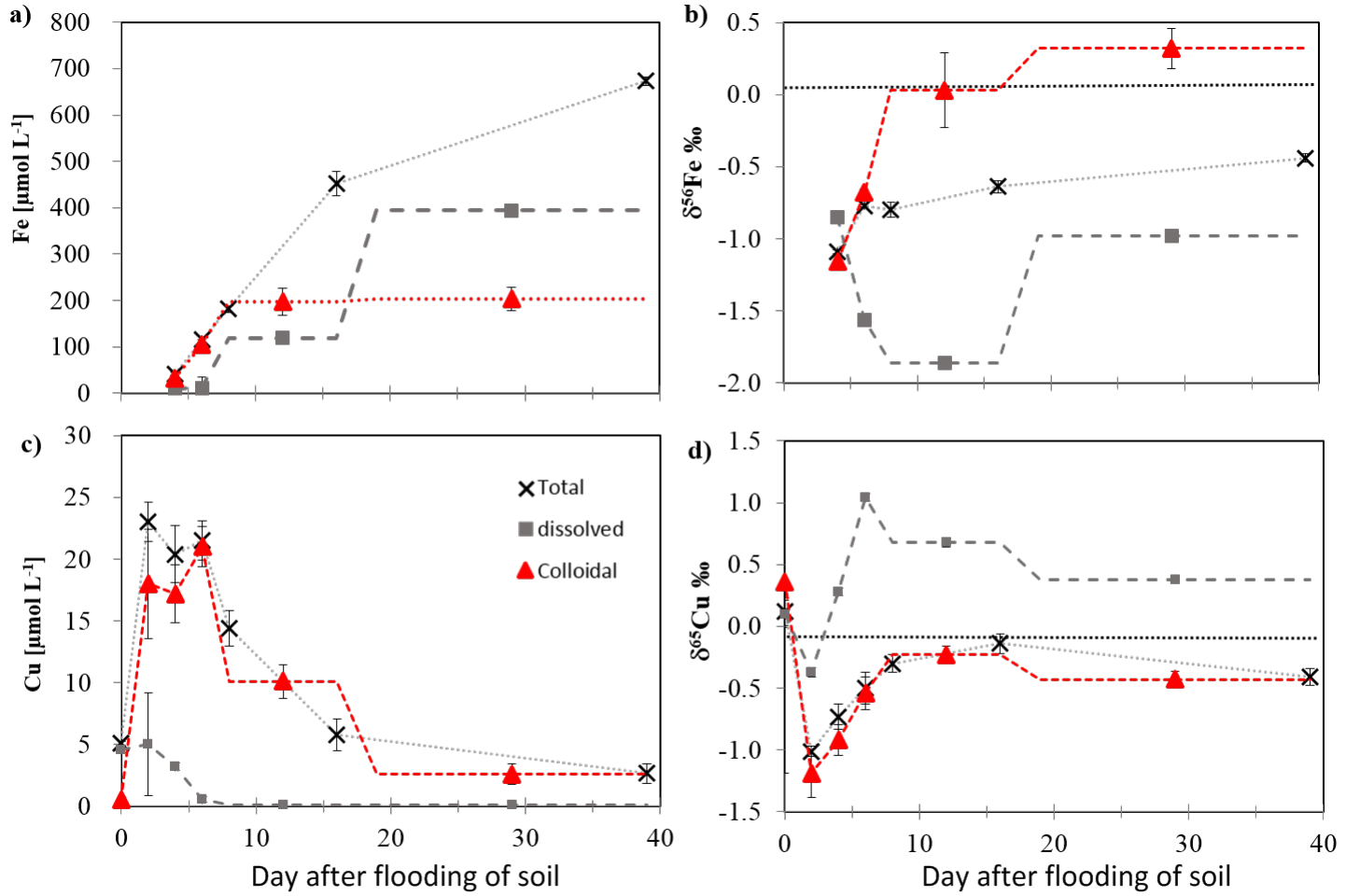

Figure 2 Temporal variation in a) Fe concentration, b) Fe isotope compositions, c) Cu concentration, and d) Cu isotope compositions during 40 days of flooding. Connection lines of the single data points are displayed to guide the eye. Plateau-like connection lines for Fe and Cu are displayed because of the pooling of the samples from different days. So every step corresponds to one sample. In Panels b and d, the dashed horizontal lines show the δ^{56}Fe (0.04±0.01‰) and δ^{65}Cu (-0.08±0.04‰) values of the bulk soil, respectively. Vertical bars in Panels a and c indicate SD of concentrations from triplicate microcosm experiments. Vertical bars in Panels b and d indicate 2SD for isotope values. Error bars are smaller than the symbols unless visible. Please note the different scales.

4. Discussion

4.1. Fe isotopes

After the flooding of soils, oxygen is consumed and electrons are released by microorganisms gaining energy from oxidation of organic matter. When the dissolved oxygen is used up, the electrons are transferred to alternative electron acceptors (Lovley, 1991). Iron (oxyhydr)oxides become the dominant alternative electron acceptors in flooded soils at sufficiently low E_h (< 150 mV). In our experiment, the E_h value decreased quickly, reached 90 mV four days after flooding and stabilized around 0 mV afterwards (Abgottspon et al., 2015). This decrease potentially triggers DIR, which is reflected in the temporal course of the total Fe concentration and δ^{56}Fe value in solution in our experiment (Figure 3) and agrees with findings of Crosby et al. (2007), Johnson et al. (2005), but also with abiotic reduction reactions (Wiederhold et al., 2006).

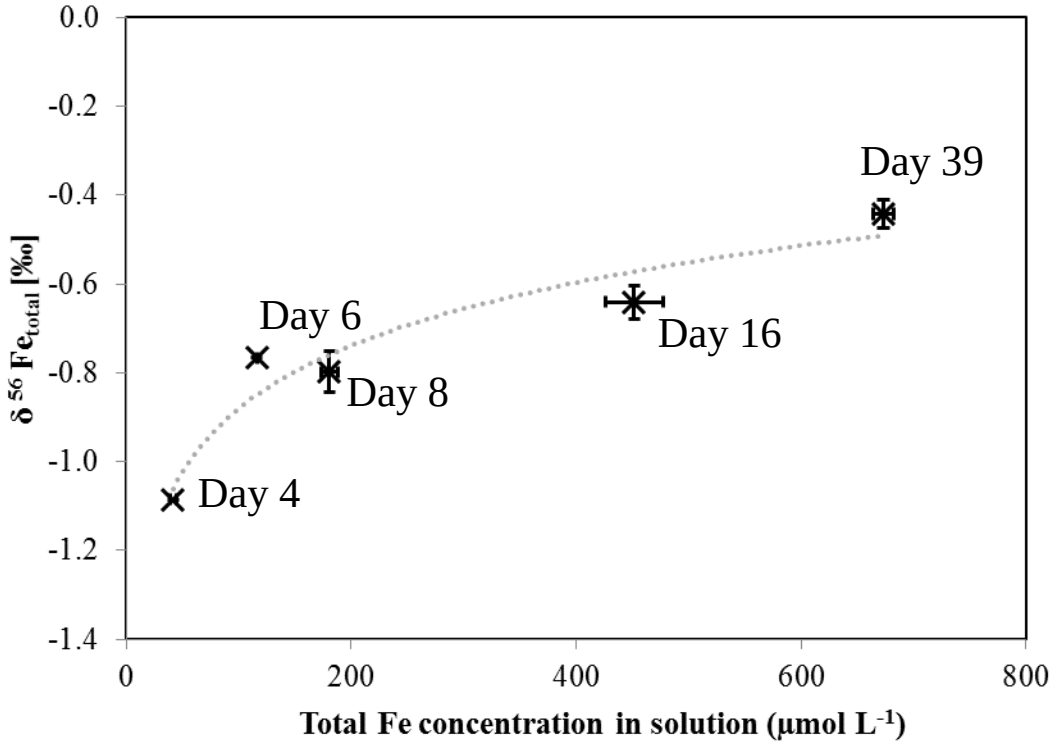

Figure 3 δ^{56}Fe values of total Fe in solution as a function of Fe concentrations during 40 days of flooding. Bars indicate SD of Fe concentrations from triplicate microcosm experiments and 2SD of Fe isotope compositions. Error bars are smaller than the symbols unless visible. The dotted line represents a logarithmic trend line.

From days 2-10, nearly all Fe in solution was Fe^{2+}, while the contribution of Fe^{2+} to total Fe in solution decreased after day 10 (Fig. 1), which is similar to the increase in Fe^{3+} concentrations in solution reported by Schuth et al. (2015). After day 19, total dissolved Fe showed higher concentrations than Fe^{2+}, indicating the presence of Fe^{3+} even in the dissolved phase. Because the solubility of Fe^{3+} is very low, this finding may only be explained by small Fe^{3+} colloids, which passed through the 0.02 µm filter (and are therefore operationally defined as dissolved species), or by the complexation of Fe^{3+} by organic substances, forming soluble complexes. Another possible explanation might be an analytical complication in the determination of the Fe^{2+} concentrations. If the Fe colloids at the end of the experiment did not fully dissolve when the sulphuric acid was added, the Fe^{2+} concentration might have been underestimated.

The pooling of the samples from different days, which was necessary because of the low Fe concentrations at the beginning of the experiment and low dissolved Cu concentrations at the end of the experiment, limit the temporal information of the Fe data. Therefore, we focus the further discussion on the Fe colloid release under anoxic conditions in soils, a process for which no Fe isotope data have yet been reported. The colloidal release plays an important role in our carbonatic floodplain soil. Up to 90% of the Fe was released in colloidal form on day 6 (Table S3; Abgottspon et al., 2015). Even in the later phase of the experiment (after day 10), colloidal Fe still accounted for 20-50% of total Fe in solution (Figure 2a). The lack of colloidal organic carbon and Al in solution (Abgottspon et al., 2015) indicate no co-mobilisation with OM or colloidal soil constituents like clay minerals, but rather Fe to be the main component of the

colloids (Table S2, S3). At the beginning of the experiment, total Fe and Fe^{2+} concentrations in solution were identical, highlighting that colloids consisted of reduced Fe and are not Fe (oxyhydr)oxides released into soil solution (Figure 1). The colloidal Fe pool had low $\delta^{56}Fe$ values at the beginning, hence supporting the idea of precipitation from reduced light Fe^{2+}_{aq} rather than mobilization by deflocculation of ferrihydrite, which should have a more positive value (span of the amorphous Fe oxide fraction in hydromorphic and oxic soils approx. -0.7 to 0.4 ‰; Guelke et al., 2010; Schuth et al., 2015; Wiederhold et al., 2007a; Wiederhold et al., 2007b) compared to the colloidal fraction on day 4 of our experiment (-1.16±0.04‰). Indeed, the initial $\Delta^{56}Fe_{dissolved\text{-}colloidal}$ value was positive and fitted the values reported for siderite precipitation in laboratory experiments ($\Delta^{56}Fe_{dissolved\text{-}siderite}$ values between 0.0 and 0.9‰; Johnson et al., 2005; Wiesli et al., 2004) and similar to that of lake sediments with supposed siderite precipitation (Figure 4a, Teutsch et al., 2009). However, when looking at the proposed $\Delta^{56}Fe_{dissolved\text{-}colloidal}$ value, it has to be kept in mind that isotopic fractionation of Fe in solution can also be influenced by interactions with the solid Fe pool in soil. Dissolved Fe^{2+} released by DIR might be sorbed to Fe (oxyhydr)oxide surfaces in soil and undergo electron transfer-atom exchange reactions, a process which influences the $\delta^{56}Fe$ value in solution (Crosby et al., 2005; 2007) and might also affect the $\Delta^{56}Fe_{dissolved\text{-}colloidal}$ values.

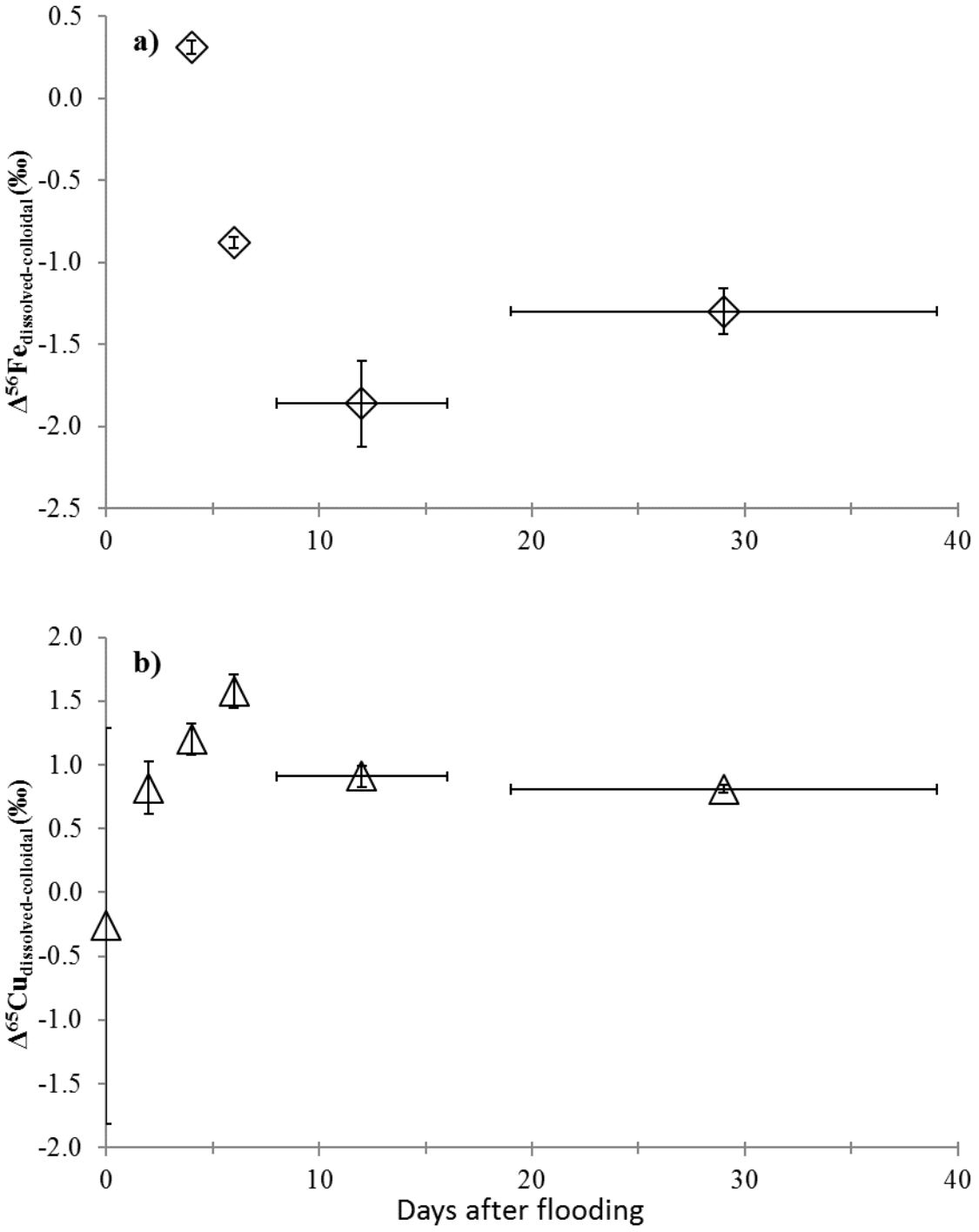

Figure 4 Temporal variations in apparent isotopic fractionation between dissolved and colloidal a) Fe and b) Cu. Horizontal error bars represent the time interval of the pooled samples. Vertical error bars represent the 2SD calculated according to Equations 3-5.

Abgottspon et al. (2015), suggested siderite precipitation from day 8 on in the same experiment. However, there is a time gap between the positive $\Delta^{56}Fe_{dissolved\text{-}colloidal}$ on day 4 and the proposed siderite precipitation. Furthermore, a confirmation of siderite formation or the precipitation of other minerals by XRD analysis was not possible because of the low mass of colloidal material on the filters and interference of the filter material (an alumina-based membrane).

Siderite can be formed by the reaction between Fe^{2+} produced by DIR and HCO_3^- produced by microbial oxidation of organic matter (Mansfeldt et al., 2012; Wiesli et al., 2004). In our soil, high concentrations of inorganic carbon in solution (10 mmol L^{-1} on day 4, Abgottspon et al., 2015) might cause a precipitation of $FeCO_3$ directly from dissolved Fe^{2+} and HCO_3^- in solution at the beginning of the experiment. This is in agreement with the presence of colloidal inorganic carbon between days 2-19 of the experiment (Abgottspon et al., 2015), a dominance of colloidal Fe and the fact that total Fe in solution was Fe^{2+} until day 10 of the experiment. Therefore, even if we have no spectroscopic proof for siderite formation, we consider siderite to be the most likely Fe mineral in colloidal Fe based on solution chemistry, isotope results and previous findings (Abgottspon et al., 2015; Du Laing et al., 2009; Mansfeldt et al., 2012; Wiesli et al., 2004). However, already on day 6, the $\Delta^{56}Fe_{dissolved\text{-}colloidal}$ changed, which may be explained by the following scenarios:

1. **Changing colloid mineralogy**. Mineralogy of the colloids may change with time, depending on changing solution chemistry and microbial community (Fulda et al., 2013; Roh et al., 2003). As an example, siderite and magnetite are formed in similar environments depending on the composition of the surrounding air and dissolved gases, the presence or absence of the carbonic acid-hydrogencarbonate buffer, pH, incubation temperature, type of

substrate, incubation time, and bacteria species (Roh et al., 2003). Sulfate reduction might induce formation of Fe sulfides (Borch et al., 2010). The change from Fe^{2+} to Fe^{3+} in the soil solution and thus changing proportions of Fe^{2+} and Fe^{3+} in the dissolved and colloidal phases might explain the variations in the $\Delta^{56}Fe_{dissolved\text{-}colloidal}$ values. Furthermore, the big gap between total Fe and total Fe^{2+} indicate that colloids change from a Fe^{2+} dominated mineral to a mineral containing also Fe^{3+}. Observed $\Delta^{56}Fe_{dissolved\text{-}colloidal}$ values are consistent with those expected for a number of Fe minerals like e.g., mackinawite or magnetite (Frierdich et al., 2014; Guilbaud et al., 2011; Johnson et al., 2005; Wu et al., 2011).

2. **Sorption and electron transfer-atom exchange reactions**. The shift to lower $\Delta^{56}Fe_{dissolved\text{-}colloidal}$ values can also be caused by sorption and possibly electron transfer-atom exchange reactions at the surface of the colloids or soil components (Crosby et al., 2005; 2007, Liu et al., 2015). The divalent dissolved Fe can be sorbed on these surfaces and electron transfer-atom exchange reactions may occur, which change isotopic signatures of Fe in solution (e.g., Frierdich et al., 2014). Sorption and electron transfer-atom exchange reactions on colloid surfaces would increase $\delta^{56}Fe$ values in colloids and decrease $\delta^{56}Fe$ values in solution, which is consistent with our results until day 16. However, also sorption to Fe oxy(hydr)oxide surfaces in the soil and electron transfer-atom exchange reactions, might explain a significant part of the observed $\delta^{56}Fe$ variation in the solution (Reddy et al., 2015). After 16 days of flooding, the shift of dissolved Fe to higher $\delta^{56}Fe$ values can be attributed to an isotopic pool size effect caused by proceeding DIR and the growth of the dissolved relative to the colloidal Fe fraction (Figure 2b).

However, the changing $\delta^{56}Fe$ values together with the increasing or constant colloid concentration, indicated that new Fe colloids were formed throughout, while the concentrations of Cu colloids steadily decreased probably because of aggregation and sedimentation.

In a recent experiment, the same soil was incubated under the same experimental conditions and changes in the partitioning of Fe into five operatively defined fractions (F1–F5; NH_4NO_3-extractable, NaOAc-extractable, NH_4Ox-extractable, hot H_2O_2/NH_4OAc-extractable and residual fractions, respectively) were investigated (Abgottspon et al., 2015). At the beginning of the experiment 81 % of the Fe in the soil was in the residual fraction which is supposed to consist mainly of silicate-bound Fe and crystalline Fe (oxyhydr)oxides, the second important fraction was the oxalate-extractable fraction (15 %, amorphous Fe oxides), while the other fractions had minor importance (< 3 %). Over the time of the incubation, Fe concentrations in F1-F4 increased, indicating a substantial redistribution of Fe, which is only partly mirrored in the solution chemistry.

A variation in solid phase $\delta^{56}Fe$ values of up to 0.93‰ was reported for soils which are seasonally or permanently water-saturated (Fekiacova et al., 2013; Liu et al., 2014b; Mansfeldt et al., 2012; Schuth et al., 2015; Wiederhold et al., 2007a). This can be attributed to the mobilization of reduced isotopically light Fe, which might be leached, leaving the soil enriched in heavier Fe isotopes (Schuth and Mansfeldt, 2016). The fractionation follows an apparent Rayleigh-type behavior with smaller fractionation factors in soils compared to experimentally found values, because of additional processes (e.g., organic complexation and reprecipitation) occurring in the complex soil system (Garnier et al. 2017, Thompson et al., 2007). In contrast, most soils that developed under oxic conditions only display a small variation in bulk solid phase $\delta^{56}Fe$ values of 0.08‰ (Podzols show variations in $\delta^{56}Fe$ values of up to 0.6‰; Poitrasson et al.,

514 2008; Wiederhold et al., 2007b). In agreement with these findings, we observed a release of light
515 Fe into the soil solution ranging from -1.1‰ to -0.4‰ (Figure 2b). The evolution of the δ^{56}Fe
516 values in total Fe during our experiment showed a time dependency with low δ^{56}Fe values
517 shortly after flooding which successively approached bulk soil values with increasing time of
518 flooding.

519 These findings agree with the interpretation of the variation in δ^{56}Fe values of total Fe in the
520 water of the Rio Negro River, where a substantial temporal variation was observed (dos Santos
521 Pinheiro et al., 2014). In Rio Negro River water, the lowest δ^{56}Fe values were coupled to strong
522 rain events, which cause a reductive mobilization of Fe from the soils in the river catchment
523 (Bergquist and Boyle, 2006). Hence, colloidal Fe release in certain anoxic soils significantly
524 affects the temporal isotopic variability of the colloidal fraction. For a detailed understanding of
525 the processes causing the isotopic changes in the colloid fraction, further investigation of the
526 associated processes and mineralogy will be needed which is beyond the scope of this study.

527 Overall, the agreement of the results from our microcosm experiment and field observations
528 confirms that such experiments can be used for future research into Fe isotopic behavior in
529 anoxic soils. A big advantage of the microcosms is that soil solution samples can be extracted
530 under controlled oxygen-free conditions and allow e.g., for the separation of colloids from
531 dissolved Fe in anoxic samples or photometric Fe^{2+} analysis. This separation is hardly possible
532 under oxic field conditions as reduced Fe^{2+} will almost immediately precipitate as Fe
533 (oxyhydr)oxides when coming in contact with the atmosphere. In spite of the limitations of our
534 study because we had to pool bulk samples of several dates and the lack of direct
535 characterization of the mineral phases, our results indicate that the Fe release in colloidal form

536 contributes substantially to total Fe concentrations and δ^{56}Fe values in solution and thus to Fe
537 mobility in our study soil.
538
539 **4.2. Cu isotopes**
540 The initial apparent isotopic fractionation between Cu in solution (total, dissolved and
541 colloidal) and in bulk soil was small (Figure 2d). With increasing time after flooding, the
542 fractionation between bulk soil and solution and between dissolved and colloidal Cu species in
543 solution increased, with total and colloidal fraction becoming lighter and the dissolved fraction
544 becoming heavier. Relating the Cu isotope ratios to a similar experiment in which Cu speciation
545 was investigated by XAS on a polluted soil from the River Mulde in Germany, offers a possible
546 explanation for most of the observed isotope fractionations. The Cu concentration peak on day 2
547 and the strong shift to negative δ^{65}Cu values of total Cu in solution could be caused by Cu-
548 carrying bacteria cells which were dominating the colloidal phase in studies with other soils
549 (Hofacker et al., 2013; Weber et al., 2009a). The simultaneously observed heavy Cu isotope ratio
550 of the remaining Cu in solution would then be the consequence of previous preferential uptake of
551 ^{63}Cu by the bacteria (Navarette et al., 2011; Pokrovsky et al., 2008), Cu reduction in the cell and
552 the change to trigonal coordination (Weber et al., 2009a). The shift in δ^{65}Cu values between
553 dissolved and colloidal Cu was similar to previously reported Cu isotope fractionation that was
554 linked to the uptake of Cu into bacteria with $\Delta^{65}Cu_{(solution\text{-}bacteria)}$ values between +1.0‰ and
555 +4.4‰ (Navarette et al., 2011). The change of δ^{65}Cu values in solution between days 2 and 6,
556 while total Cu concentrations remained stable, can only be explained by the exchange of solution
557 Cu with solid soil Cu pools. The shift to higher δ^{65}Cu values from -1.01±0.04‰ to -0.50±0.13‰
558 in total Cu in solution requires the removal of isotopically light Cu from solution and/or release

559 of heavy Cu into solution. In the experiments of Hofacker et al. (2013) and Weber et al. (2009a),
560 bacteria released Cu^{+}, which disproportioned into Cu^{2+}, released into solution, and zero-valent
561 Cu (Cu^{0}) colloids, in this phase of the incubation. In solution, Cu^{2+} released from bacteria was
562 partly reduced and precipitated together with the already present Cu in soil solution and
563 exchangeable Cu from the solid soil as Cu_xS (Weber et al., 2009b). If this process also occurred
564 in our experiment the Cu_xS would be a mixture of soil Cu and solution Cu and would probably
565 carry a heavier isotopic signal than that of the Cu in the bacteria. After day 6 with the onset of
566 sulfate reduction (Table S2, Abgottspon et al., 2015), Cu isotope composition and apparent
567 fractionation between dissolved and colloidal Cu stabilized (average values of $\delta^{65}Cu$ = -
568 0.29±0.15‰ and $\Delta^{65}Cu_{dissolved\text{-}colloidal}$ = 0.87±0.09‰) despite decreasing Cu concentrations in
569 solution. These findings indicate that the further decrease of colloidal Cu was caused by a
570 progressive aggregation and sedimentation of colloids, which does not cause a pronounced
571 isotopic fractionation (Figure 4b). Even if the results from the soil investigated by Hofacker et al.
572 (2013) and Weber et al. (2009a) cannot be directly transferred to our soil because of the acid soil
573 used by these authors and our slightly alkaline soil, Abgottspon et al. (2015) showed that in our
574 soil decreasing metal mobilization paralleled increasing sulfate reduction. However, the fact that
575 we did not observe colloidal organic carbon at the beginning of the experiment (Table S2)
576 disagrees with the findings of bacterial release causing the increase of colloidal Cu at the
577 beginning of the experiment (Hofacker et al., 2013; Weber et al. 2009a). Assuming a C/Cu (w/w)
578 ratio of about 4000 as described for methanogenic bacteria (Scherer et al., 1983), a bacterial
579 release causing 23 µmol Cu L^{-1} on day 2 should be clearly visible also in colloidal C (approx.
580 500 mmol L^{-1}). Even if the strong variation of Cu concentrations in bacteria is taken into

account, the colloidal C concentration should be clearly higher than the measured 0.2 mmol L^{-1} C_{coll} (Table S2), if bacteria caused the colloidal Cu concentration on day 2.

One might hypothesize that the reported changes of Cu redox states (Weber et al., 2009a) explain much of the observed $\Delta^{65}Cu_{dissolved\text{-}colloidal}$ values in soil solution, which are 0.82±0.20‰ on day 2, when Cu is supposed to occur as Cu^{+} and reach a maximum value of 1.58±0.13‰ on day 6 as a result of the presumed dominance of Cu^{0}. After sulfate reduction on days 6-8 (Table S1), $\Delta^{65}Cu_{dissolved\text{-}colloidal}$ values changed back to 0.81±0.03‰, in line with the assumption that Cu^{+} was the dominant Cu species (Weber et al., 2009a; Figure 4b). However, it is not clear, if the same redox transformations as described by Weber et al. (2009a) occur in the soil used in our experiment. Generally, the isotopic fractionation associated with abiotic oxidative leaching of reduced Cu minerals (chalcocite, chalcopyrite, enargite) is in the range of $\Delta^{65}Cu_{aq\text{-}mineral}$ = 0 to 2.7‰ in laboratory experiments and field surveys (Fernandez and Borrok, 2009; Kimball et al., 2008; Mathur et al., 2005) and agree well with theoretical estimations stating that Cu(I) complexes preferentially enrich ^{63}Cu and their precipitation results in the enrichment of ^{65}Cu in the fluid (Fuji et al., 2013). This pattern supports the interpretation that the observed $\Delta^{65}Cu_{dissolved\text{-}colloidal}$ values in our experiment are caused by precipitation of reduced colloidal Cu species. However, fractionation has been reported to be irrelevant or even in the opposite direction in the presence of bacteria (Kimball et al., 2008, Mathur et al., 2005). The latter has been explained with the accumulation of heavy isotopes on the bacteria and preferential precipitation of heavy Cu on bacteria surfaces. The biotic induced isotope fractionation is counteracting the isotope fractionation introduced by abitic redox processes. Thus in a system with reducing conditions and bacteria the $\delta^{65}Cu$ values in solution are determined by the balance of Cu released abiotically and Cu that interacts with the cells and biotic precipitates (Mathur et

al., 2005, Kimball et al., 2008). If we transfer the latter findings to our $\Delta^{65}Cu_{dissolved\text{-}colloidal}$ values, this might indicate that abiotic reduction rather that bacterial Cu precipitation is governing colloid formation. However, the influence of microorganisms as well as other soil process (e.g. organic complexation or reprecipitation as described by Thompson et al., 2007 for Fe), might decrease the apparent fractionation in our soil, compared to experimentally determined fractionation factors in less complex systems (e.g., Fernandez and Borrok, 2009; Zhu et al., 2002) .

In a recent experiment (Kusonwiriyawong et al., 2016), we determined the changes in Cu partitioning and the $\delta^{65}Cu$ values in five fractions of a sequential extraction (F1–F5; NH_4NO_3-extractable, NaOAc-extractable, NH_4Ox-extractable, hot H_2O_2/NH_4OAc-extractable and residual fractions, respectively) in the same soils that we used in this study. We found that in the dry soil, $\delta^{65}Cu$ values in F1–F4 followed the estimated bonding strengths of Cu in the respective fractions, indicating equilibrium distribution of Cu at the beginning of the experiment. After flooding, Cu concentrations decreased in F1–F3 and increased in F4–F5. Overall, 73% of the total Cu was redistributed among the five studied fractions. The strongest variations in $\delta^{65}Cu$ values occurred in F3 (0.09±0.07‰ to 1.43±0.13‰) and F4 (−0.24±0.07‰ to 0.55±0.07‰), while flooding had no or small effects on the $\delta^{65}Cu$ values of F1, F2 and F5. So even if F1 should be the Cu pool, which interacts most strongly with the solution, it did not mirror the shifts of the dissolved fractions in this experiment. The results from Kusonwiriyawong et al. (2016) suggest a direct transfer of Cu from F3 to F4 because both concentration changes and changes in $\delta^{65}Cu$ values were balanced between the two fractions. The responses of Cu partitioning and $\delta^{65}Cu$ values to flooding are in line with the formation of CuxS or other reduced Cu species and the reduction of Cu associated with Fe (oxyhydr)oxides.

627 One factor which can only be traced with the used isotopic approach is the exchange of
628 Cu in solution with solid soil Cu, which is most pronounced between days 2-6. On day 8, the
629 total δ^{65}Cu value of the soil solution showed good agreement with that of Fraction 4 of the
630 sequential extraction of the solid soil by Kusonwiriyawong et al. (2016) on day 7, which is
631 supposed to represent reduced Cu phases. The agreement in these two δ^{65}Cu values supports the
632 assumption, that at this time colloidal Cu in solution and solid soil Cu are coupled. However, the
633 Cu isotope signatures in Fraction 4 in the solid soil changed to positive values (0.55±0.07‰) on
634 day 35, while dissolved Cu still showed negative δ^{65}Cu values and did not change significantly
635 between days 8 and 39. This suggests that after the initial peak Cu colloid concentration, colloid
636 formation and exchange with the soil stopped, while aggregation in solution decreased the Cu
637 colloid concentration.

638 Babcsanyi et al. (2014) and Bigalke et al. (2010b, 2011, 2013) investigated different oxic
639 and anoxic soils and wetland systems and found that Cu isotope signatures were isotopically
640 heavier in temporally flooded soils than in soils, which developed in an oxic environment. They
641 concluded that isotopically light Cu was released from flooded wetlands. Furthermore, these
642 authors suggested that leaching of reduced Cu colloids was responsible for the observed apparent
643 fractionation. This assumption is confirmed by our findings, which demonstrate a strong release
644 of light colloidal Cu shortly after flooding. Leaching of this Cu from the soil would cause the
645 described shift to heavier δ^{65}Cu values. The extent of the fractionation in real soils would depend
646 on the progress of leaching. In our study soil, the lowest δ^{65}Cu value for total Cu in solution
647 occurred on day 2. Assuming a similar δ^{65}Cu value (-1.0‰) of the total Cu released into solution
648 and leached over several redox cycles and a leaching of e.g., 10% of the initial Cu in bulk soil,
649 the total Cu in bulk soil should be isotopically shifted from initially 0 to +0.1‰.

This mobilization of Cu has to be considered in the management of polluted sites, by preventing changes of redox conditions. Especially, floodplain soils, which show high metal concentrations in many cases, might directly leach the Cu to the associated river, and thus negatively affect the river ecosystem. Because the colloids are carrying up to 100% of Cu and associated trace metals in soil solution and will strongly affect transport behavior and toxicity (Griffitt et al., 2007; Ju-Nam and Lead, 2008), the extent and stability of colloids formed in carbonatic soils need to be considered in risk assessments.

5. Conclusions

- Total $\delta^{56}Fe$ values in solution followed the pattern of DIR. The $\Delta^{56}Fe_{dissolved\text{-}colloidal}$ values indicated that dissolved Fe precipitated directly to form colloids, which accounted for 90% of total Fe at the beginning to 20% of total Fe at the end of the experiment. While siderite precipitation might be one reason for colloidal Fe formation, a change of $\Delta^{56}Fe_{dissolved\text{-}colloidal}$ values with time indicates either changes in the colloid mineralogy, or sorption and possible electron transfer-atom exchange reactions with colloidal Fe or Fe minerals in the soil solid phase. The results match previous findings from lake, river and soil environments and underline the significance of colloid formation from dissolved Fe in some anoxic soil environments. The strong changes in $\Delta^{56}Fe_{dissolved\text{-}colloidal}$ values raise new questions about formation and changes of the Fe colloid composition under anoxic conditions.
- The $\Delta^{65}Cu_{dissolved\text{-}colloidal}$ seemed to be mainly driven by Cu redox state. The $\delta^{65}Cu$ values indicated a strong exchange of colloidal Cu with solid soil Cu and a decoupling of these two pools with beginning sulfate reduction and decreasing Cu concentrations in solution.

673 The comparison of the experimental results with previous findings from hydromorphic
674 soils and wetlands indicates that Cu colloid formation might be an important factor
675 driving Cu leaching in these environments. Therefore, Cu colloid formation should be
676 accounted for in risk assessment of e.g., polluted floodplain soils and similar
677 environments.

678 In this study, the first results of Fe and Cu isotopic composition of colloids forming in anoxic
679 soil environments are presented. Both elements are redox sensitive and probably undergo
680 reduction, but show distinctly different temporal concentration and isotopic patterns. Both
681 elements have a considerable colloidal component in common. Colloidal Fe and Cu might cause
682 colloidal co-mobilization of a line of other potential toxic elements in soils. Furthermore,
683 colloidal properties need to be considered in toxicity and mobility assessments.

684

685 **Acknowledgements**

686 We thank the group of Isotope Geology of the University of Berne, Klaus Mezger, Thomas
687 Nägler, Igor Villa and Gabriela Balzer for access to the clean room and support. We thank the
688 AE Michael Böttcher and the two reviewers Ryan Mathur and Jan Wiederhold for their
689 constructive comments, which considerably improved the manuscript. We also thank the
690 Agricultural Research Development Agency (Public Organization), ARDA, Thailand, for
691 funding Charirat Kusonwiriyawong.

692

693 **Supporting Material**

694 Supporting material for this manuscript is available, including soil characterization, solution
695 chemistry data and figures illustrating the experimental setup and a three isotope plot for the Fe
696 isotope analysis.
697
698

699 **References**

700 Abgottspon, F., Bigalke, M., Wilcke, W., 2015. Mobilization of trace elements in a carbonatic
701 soil after experimental flooding. Geoderma 259-260, 156-163.
702 Babcsanyi, I., Imfeld, G., Granet, M., Chabaux, F., 2014. Copper stable isotopes to trace copper
703 behavior in wetland systems. Environ. Sci. Technol. 48(10), 5520-5529.
704 Balistrieri, L.S., Borrok, D.M., Wanty, R.B., Ridley, W.I., 2008. Fractionation of Cu and Zn
705 isotopes during adsorption onto amorphous Fe(III) oxyhydroxide: Experimental mixing
706 of acid rock drainage and ambient river water. Geochim. Cosmochim. Acta 72(2), 311-
707 328.
708 Bergquist, B.A., Boyle, E.A., 2006. Iron isotopes in the Amazon River system: Weathering and
709 transport signatures. Earth Planet. Sci. Lett. 248(1-2), 54-68.
710 Bigalke, M., Kersten, M., Weyer, S., Wilcke, W., 2013. Isotopes trace biogeochemistry and
711 sources of Cu and Zn in an intertidal soil. Soil Sci. Soc. Am. J.
712 doi:10.2136/sssaj2012.0225.
713 Bigalke, M., Weyer, S., Wilcke, W., 2010a. Copper isotope fractionation during complexation
714 with insolubilized humic acid. Environ. Sci. Technol. 44(14), 5496-5502.
715 Bigalke, M., Weyer, S., Wilcke, W., 2010b. Stable Copper Isotopes: A novel tool to trace copper
716 behavior in hydromorphic soils. Soil Sci. Soc. Am. J. 74(1), 60-73.
717 Bigalke, M., Weyer, S., Wilcke, W., 2011. Stable Cu isotope fractionation in soils during oxic
718 weathering and podzolation. Geochim. Cosmochim. Acta 75(11), 3119-3134.
719 Borch, T., Kretzschmar, R., Kappler, A., Van Cappellen, P., Ginder-Vogel, M., Voegelin, A.,
720 Campbell, K., 2010. Biogeochemical redox processes and their impact on contaminant
721 dynamics. Environ. Sci. Technol. 44(1), 15-23.
722 Brantley, S.L., Liermann, L., Bullen, T.D., 2001. Fractionation of Fe isotopes by soil microbes
723 and organic acids. Geology 29(6), 535-538.
724 Burton, E.D., Bush, R.T., Sullivan, L.A., Johnston, S.G., Hocking, R.K., 2008. Mobility of
725 arsenic and selected metals during re-flooding of iron- and organic-rich acid-sulfate soil.
726 Chem. Geol. 253(1-2), 64-73.
727 Butler, I.B., Archer, C., Vance, D., Oldroyd, A., Rickard, D., 2005. Fe isotope fractionation on
728 FeS formation in ambient aqueous solution. Earth and Planetary Science Letters, 236(1-
729 2): 430-442.

730 Contin, M., Mondini, C., Leita, L., De Nobili, M., 2007. Enhanced soil toxic metal fixation in
731 iron (hydr)oxides by redox cycles. Geoderma 140(1-2), 164-175.
732 Craddock, P.R., Dauphas, N., 2011. Iron Isotopic compositions of geological reference materials
733 and chondrites. Geostand. Geoanal. Res. 35(1), 101-123.
734 Crosby, H.A., Roden, E.E., Johnson, C.M., Beard, B.L., 2007. The mechanisms of iron isotope
735 fractionation produced during dissimilatory Fe(III) reduction by Shewanella putrefaciens
736 and Geobacter sulfurreducens. Geobiology 5(2), 169-189.
737 Dideriksen, K., Baker, J.A., Stipp, S.L.S., 2008. Equilibrium Fe isotope fractionation between
738 inorganic aqueous Fe(III) and the siderophore complex, Fe(III)-desferrioxamine B. Earth
739 Planet. Sci. Lett. 269(1-2), 280-290.
740 Dos Santos Pinheiro, G.M.D., Poitrasson, F., Sondag, F., Cochonneau, G., Vieira, L.C., 2014.
741 Contrasting iron isotopic compositions in river suspended particulate matter: the Negro
742 and the Amazon annual river cycles. Earth Planet. Sci. Lett. 394, 168-178.
743 Du Laing, G., Rinklebe, J., Vandecasteele, B., Meers, E., Tack, F.M.G., 2009. Trace metal
744 behaviour in estuarine and riverine floodplain soils and sediments: A review. Sci. Total
745 Environ. 407(13), 3972-3985.
746 Du Laing, G., Vanthuyne, D.R.J., Vandecasteele, B., Tack, F.M.G., Verloo, M.G., 2007.
747 Influence of hydrological regime on pore water metal concentrations in a contaminated
748 sediment-derived soil. Environ. Pollut. 147(3), 615-625.
749 Ehrlich, S., Butler, I., Halicz, L., Rickard, D., Oldroyd, A., Matthews, A., 2004. Experimental
750 study of the copper isotope fractionation between aqueous Cu(II) and covellite, CuS.
751 Chem. Geol. 209(3-4), 259-269.
752 Fehr, M.A., Andersson, P.S., Halenius, U., Morth, C.M., 2008. Iron isotope variations in
753 Holocene sediments of the Gotland Deep, Baltic Sea. Geochim. Cosmochim. Acta
754 72(3), 807-826.
755 Fekiacova, Z., Pichat, S., Cornu, S., Balesdent, J., 2013. Inferences from the vertical distribution
756 of Fe isotopic compositions on pedogenetic processes in soils. Geoderma 209, 110-118.
757 Fernandez, A., Borrok, D.M., 2009. Fractionation of Cu, Fe, and Zn isotopes during the
758 oxidative weathering of sulfide-rich rocks. Chemi. Geol. 264 (1-4), 1-12.
759 Frierdich, A.J., Beard, B.L., Scherer, M.M., Johnson, C.M., 2014. Determination of the
760 Fe(II)(aq)-magnetite equilibrium iron isotope fractionation factor using the three-isotope

761 method and a multi-direction approach to equilibrium. Earth Planet. Sci. Lett. 391, 77-
762 86.
763 Frohne, T., Rinklebe, J., Diaz-Bone, R.A., Du Laing, G., 2011. Controlled variation of redox
764 conditions in a floodplain soil: Impact on metal mobilization and biomethylation of
765 arsenic and antimony. Geoderma 160(3-4), 414-424.
766 Fujii, T., Moynier, F., Abe, M., Nemoto, K., Albarede, F., 2013. Copper isotope fractionation
767 between aqueous compounds relevant to low temperature geochemistry and biology.
768 Geochim. Cosmochim. Acta 110, 29-44.
769 Fulda, B., Voegelin, A., Ehlert, K., Kretzschmar, R., 2013. Redox transformation, solid phase
770 speciation and solution dynamics of copper during soil reduction and reoxidation as
771 affected by sulfate availability. Geochim. Cosmochim. Acta 123, 385-402.
772 Garnier, J., J-M., G., C-L., V., Akerman, A., Chmeleff, J., Ruize, R.I., Poitrasson, F., 2017. Iron
773 isotope fingerprints of redox and biogeochemical cycling in the soil-water-rice plant
774 system of a paddy field. Sci. Total Environ. 574, 1622-1632.
775 Griffitt, R.J., Weil, R., Hyndman, K.A., Denslow, N.D., Powers, K., Taylor, D., Barber, D.S.,
776 2007. Exposure to copper nanoparticles causes gill injury and acute lethality in zebrafish
777 (Danio rerio). Environ. Sci. Technol. 41(23), 8178-8186.
778 Guelke, M., von Blanckenburg, F., Schoenberg, R., Staubwasser, M., Stuetzel, H., 2010.
779 Determining the stable Fe isotope signature of plant-available iron in soils. Chem. Geol.
780 277(3-4), 269-280.
781 Guilbaud, R., Butler, I.B., Ellam, R.M., Rickard, D., Oldroyd, A., 2011. Experimental
782 determination of the equilibrium Fe isotope fractionation between Fe-aq(2+) and FeSm
783 (mackinawite) at 25 and 2 degrees C. Geochim. Cosmochim. Acta 75(10), 2721-2734.
784 Hassellov, M., von der Kammer, F., 2008. Iron oxides as geochemical nanovectors for metal
785 transport in soil-river systems. Elements 4(6), 401-406.
786 Hindersmann, I., Hippler, J., Hirner, A.V., Mansfeldt, T., 2014. Mercury volatilization from a
787 floodplain soil during a simulated flooding event. J. Soils Sed. 14(9), 1549-1558.
788 Hindersmann, I., Mansfeldt, T., 2014. Trace element solubility in a multimetal-contaminated soil
789 as affected by redox conditions. Water Air Soil Poll. 225(10).

790 Hofacker, A.F., Voegelin, A., Kaegi, R., Weber, F.A., Kretzschmar, R., 2013. Temperature-
791 dependent formation of metallic copper and metal sulfide nanoparticles during flooding
792 of a contaminated soil. Geochim. Cosmochim. Acta 103, 316-332.
793 Icopini, G.A., Anbar, A.D., Ruebush, S.S., Tien, M., Brantley, S.L., 2004. Iron isotope
794 fractionation during microbial reduction of iron: The importance of adsorption. Geology
795 32(3), 205-208.
796 Ilina, S.M., Poitrasson, F., Lapitskiy, S.A., Alekhin, Y.V., Viers, J., Pokrovsky, O.S., 2013a.
797 Extreme iron isotope fractionation between colloids and particles of boreal and temperate
798 organic-rich waters. Geochim. Cosmochim. Acta 101, 96-111.
799 Ilina, S.M., Viers, J., Lapitsky, S.A., Mialle, S., Mavromatis, V., Chmeleff, J., Brunet, P.,
800 Alekhin, Y.V., Isnard, H., Pokrovsky, O.S., 2013b. Stable (Cu, Mg) and radiogenic (Sr,
801 Nd) isotope fractionation in colloids of boreal organic-rich waters. Chem. Geol. 342, 63-
802 75.
803 IUSS Working Group WRB. 2014. World Reference Base for Soil Resources 2014. International
804 soil classification system for naming soils and creating legends for soil maps. World Soil
805 Resources Reports No. 106. FAO; Rome.
806 Johnson, C.M., Beard, B.L., Klein, C., Beukes, N.J., Roden, E.E., 2008. Iron isotopes constrain
807 biologic and abiologic processes in banded iron formation genesis. Geochim.
808 Cosmochim. Acta 72(1), 151-169.
809 Johnson, C.M., Roden, E.E., Welch, S.A., Beard, B.L., 2005. Experimental constraints on Fe
810 isotope fractionation during magnetite and Fe carbonate formation coupled to
811 dissimilatory hydrous ferric oxide reduction. Geochim. Cosmochim. Acta 69(4), 963-993.
812 Ju-Nam, Y., Lead, J.R., 2008. Manufactured nanoparticles: An overview of their chemistry,
813 interactions and potential environmental implications. Sci. Total Environ. 400(1-3), 396-
814 414.
815 Kayser, A., Presler, J., Meuli, R.G., Kägi, J., 2006. Bodenbelastungsgebiet Dornach -
816 Synthesebericht, Amt für Umwelt des Kantons Solothurn, Solothurn.
817 Kiczka, M., Wiederhold, J.G., Frommer, J., Voegelin, A., Kraemer, S.M., Bourdon, B.,
818 Kretzschmar, R., 2011. Iron speciation and isotope fractionation during silicate
819 weathering and soil formation in an alpine glacier forefield chronosequence. Geochim.
820 Cosmochim. Acta 75(19), 5559-5573.

821 Kimball, B.E., Mathur, R., Dohnalkova, A.C., Wall, A.J., Runkel, R.L., Brantley, S.L., 2009.
822 Copper isotope fractionation in acid mine drainage. Geochim. Cosmochim. Acta 73(5),
823 1247-1263.
824 Kusonwiriyawong, C., Bigalke, M., Abgottspon, F., Lazarov, M., Wilcke, W., 2016. Response of
825 Cu partitioning to flooding: A δ65Cu approach in a carbonatic alluvial soil. Chem. Geol.
826 420, 69-76.
827 Lazarov, M., Horn, I., 2015. Matrix and energy effects during in-situ determination of Cu isotope
828 ratios by ultraviolet-femtosecond laser ablation multicollector inductively coupled plasma
829 mass spectrometry. Spectrochim. Acta Part B 111, 64–73.
830 Li, D.D., Liu, S.A., Li, S.G., 2015. Copper isotope fractionation during adsorption onto kaolinite:
831 Experimental approach and applications. Chem. Geol. 396, 74-82.
832 Liu, S.A., Li, D.D., Li, S.G., Teng, F.Z., Ke, S., He, Y.S., Lu, Y.H., 2014a. High-precision
833 copper and iron isotope analysis of igneous rock standards by MC-ICP-MS. J. Anal. At.
834 Spectrom. 29(1), 122-133.
835 Liu, S.A., Teng, F.Z., Li, S.G., Wei, G.J., Ma, J.L., Li, D.D., 2014b. Copper and iron isotope
836 fractionation during weathering and pedogenesis: Insights from saprolite profiles.
837 Geochim. Cosmochim. Acta 146, 59-75.
838 Liu, K., Wu, L.L., Couture, R.M., Li, W.Q., Van Cappellen, P., 2015. Iron isotope fractionation
839 in sediments of an oligotrophic freshwater lake. Earth and Planetary Science Letters, 423:
840 164-172.
841 Lovley, D.R., 1991. Dissimilatory Fe(Iii) and Mn(Iv) reduction. Microbiol. Rev. 55(2), 259-287.
842 Malinovsky, D., Stenberg, A., Rodushkin, I., Andren, H., Ingri, J., Ohlander, B., Baxter, D.C.,
843 2003. Performance of high resolution MC-ICP-MS for Fe isotope ratio measurements in
844 sedimentary geological materials. J. Anal. At. Spectrom. 18(7), 687-695.
845 Mansfeldt, T., Overesch, M., 2013. Arsenic mobility and speciation in a gleysol with petrogleyic
846 properties: A field and laboratory approach. J. Environ. Qual. 42(4), 1130-1141.
847 Mansfeldt, T., Schuth, S., Hausler, W., Wagner, F.E., Kaufhold, S., Overesch, M., 2012. Iron
848 oxide mineralogy and stable iron isotope composition in a Gleysol with petrogleyic
849 properties. J. Soils Sed. 12(1), 97-114.

Mathur, R., Ruiz, J., Titley, S., Liermann, L., Buss, H., Brantley, S., 2005. Cu isotopic fractionation in the supergene environment with and without bacteria. Geochim. Cosmochim. Acta, 69 (22), 5233-5246.

Mikutta, C., Wiederhold, J.G., Cirpka, O.A., Hofstetter, T.B., Bourdon, B., von Gunten, U., 2009. Iron isotope fractionation and atom exchange during sorption of ferrous iron to mineral surfaced. Geochim. Cosmochim. Acta 73, 1795-1812.

Moeller, K., Schoenberg, R., Pedersen, R.B., Weiss, D., Dong, S.F., 2012. Calibration of the new certified reference materials ERM-AE633 and ERM-AE647 for copper and IRMM-3702 for zinc isotope amount ratio determinations. Geostand. Geoanal. Res. 36(2), 177-199.

Morgan, J.L.L., Wasylenki, L.E., Nuester, J., Anbar, A.D., 2010. Fe isotope fractionation during equilibration of Fe-organic complexes. Environ. Sci. Technol. 44(16), 6095-6101.

Mulholland, D.S., Poitrasson, F., Shirokova, L.S., Gonzalez, A.G., Pokrovsky, O.S., Boaventura, G.R., Vieira, L.C., 2015. Iron isotope fractionation during Fe(II) and Fe(III) adsorption on cyanobacteria. Chem. Geol. 400, 24-33.

Navarette, J.N., Borrok, D.M., Viveros, M., Ellzey, J.T., 2011. Copper isotope fractionation during surface adsorption and intracellular incorporation by bacteria. Geochim. Cosmochim. Acta 75, 784-799.

Oeser, M., Weyer, S., Horn, I., Schuth, S. 2014. High-precision Fe and Mg isotope ratios of silicate reference glasses determined in situ by femtosecond LA-MC-ICP-MS and by solution nebulisation MC-ICP-MS, Geostand. Geoanalit. Res. 37, 311-328.

Poitrasson, F., Viers, J., Martin, F., Braun, J.J., 2008. Limited iron isotope variations in recent lateritic soils from Nsimi, Cameroon: Implications for the global Fe geochemical cycle. Chem. Geol. 253(1-2), 54-63.

Pokrovsky, O.S., Vim, J., Emnova, E.E., Kompantseva, E.I., Freydier, R., 2008. Copper isotope fractionation during its interaction with soil and aquatic microorganisms and metal oxy(hydr) oxides: Possible structural control. Geochim. Cosmochim. Acta 72(7), 1742-1757.

Ponnamperuma, F.N., 1972. The chemistry of submerged soils. Advances in Agronomy 24, 29-94.

Ratering, S., Schnell, S., 2000. Localization of iron-reducing activity in paddy soil by profile studies. Biogeochemistry 48(3), 341-365.

881 Reddy, T.R., Frierdich, A.J., Beard, B.L., Johnson, C.M., 2015. The effect of pH on stable iron
882 isotope exchange and fractionation between aqueous Fe(II) and goethite. Chemical
883 Geology, 397: 118-127.
884 Roh, Y., Zhang, C.L., Vali, H., Lauf, R.J., Zhou, J., Phelps, T.J., 2003. Biogeochemical and
885 environmental factors in Fe biomineralization: Magnetite and siderite formation. Clays
886 Clay Miner. 51(1), 83-95.
887 Ryan, B.M., Kirby, J.K., Degryse, F., Scheiderich, K., McLaughlin, M.J., 2014. Copper isotope
888 fractionation during equilibration with natural and synthetic ligands. Environ. Sci.
889 Technol. 48(15), 8620-8626.
890 Scherer, P., Lippert, H., Wolff, G., 1983. Composition of the major elements and trace elements
891 of ten methanogenic bacteria determined by Inductively-Coupled Plasma Emission-
892 Spectrometry. Biol. Trace Elem. Res. 5(3), 149-163.
893 Schuth, S., Hurraß, J., Münker, C., Mansfeldt, T., 2015. Redox-dependent fractionation of iron
894 isotopes in suspensions of a groundwater-influenced soil. Chem. Geol. 392, 74-86.
895 Schuth, S., Mansfeldt, T., 2016. Iron isotope composition of aqueous phases of a lowland
896 environment. Environ. Chem. 13(1), 89-101.
897 Tadanier, C.J., Schreiber, M.E., Roller, J.W., 2005. Arsenic mobilization through microbially
898 mediated deflocculation of ferrihydrite. Environ. Sci. Technol. 39(9), 3061-3068.
899 Taylor, R.M., 1980. Formation and properties of Fe(Ii)Fe(Iii) hydroxy-carbonate and its possible
900 significance in soil formation. Clay Miner. 15(4), 369-382.
901 Taylor, J.R. 1997. An introduction to error analysis: the study of uncertainties in physical
902 measurements, 2nd ed. University Science Books, Sausalito, CA.
903 Teutsch, N., Schmid, M., Muller, B., Halliday, A.N., Burgmann, H., Wehrli, B., 2009. Large iron
904 isotope fractionation at the oxic-anoxic boundary in Lake Nyos. Earth Planet. Sci. Lett.
905 285(1-2), 52-60.
906 Teutsch, N., von Gunten, U., Porcelli, D., Cirpka, O.A., Halliday, A.N., 2005. Adsorption as a
907 cause for iron isotope fractionation in reduced groundwater. Geochim. Cosmochim. Acta
908 69(17), 4175-4185.
909 Thompson, A., Ruiz, J., Chadwick, O.A., Titus, M., Chorover, J., 2007. Rayleigh fractionation of
910 iron isotopes during pedogenesis along a climate sequence of Hawaiian basalt. Chem.
911 Geol. 238 (1-2), 72-83.

912 Vance, D., Archer, C., Bermin, J., Perkins, J., Statham, P.J., Lohan, M.C., Ellwood, M.J., Mills,
913 R.A., 2008. The copper isotope geochemistry of rivers and the oceans. Earth Planet. Sci.
914 Lett. 274(1-2), 204-213.
915 Weber, F.A., Voegelin, A., Kaegi, R., Kretzschmar, R., 2009a. Contaminant mobilization by
916 metallic copper and metal sulphide colloids in flooded soil. Nat. Geosci. 2(4), 267-271.
917 Weber, F.A., Voegelin, A., Kretzschmar, R., 2009b. Multi-metal contaminant dynamics in
918 temporarily flooded soil under sulfate limitation. Geochim. Cosmochim. Acta 73(19),
919 5513-5527.
920 Weyer, S., Schwieters, J., 2003. High precision Fe isotope measurements with high mass
921 resolution MC-ICPMS. Int. J. Mass. Spectrom. 226, 355–368.
922 Weyer, S., Anbar, A.D., Brey, G.P., Munker, C., Mezger, K., Woodland, A.B., 2005. Iron
923 isotope fractionation during planetary differentiation. Earth Planet. Sci. Lett. 240(2), 251-
924 264.
925 Wiederhold, J.G., Kraemer, S.M., Teutsch, N., Borer, P.M., Halliday, A.N., Kretzschmar, R.,
926 2006. Iron isotope fractionation during proton-promoted, ligand-controlled, and reductive
927 dissolution of goethite. Environ. Sci. Technol. 40(12), 3787-3793.
928 Wiederhold, J.G., Teutsch, N., Kraemer, S.M., Halliday, A.N., Kretzschmar, R., 2007a. Iron
929 isotope fractionation during pedogenesis in redoximorphic soils. Soil Sci. Soc. Am. J.
930 71(6), 1840-1850.
931 Wiederhold, J.G., Teutsch, N., Kraemer, S.M., Halliday, A.N., Kretzschmar, R., 2007b. Iron
932 isotope fractionation in oxic soils by mineral weathering and podzolization. Geochim.
933 Cosmochim. Acta 71(23), 5821-5833.
934 Wiesli, R.A., Beard, B.L., Johnson, C.M., 2004. Experimental determination of Fe isotope
935 fractionation between aqueous Fe(II), siderite and "green rust" in abiotic systems. Chem.
936 Geol. 211(3-4), 343-362.
937 Wu, L.L., Beard, B.L., Roden, E.E., Johnson, C.M., 2011. Stable iron isotope fractionation
938 between aqueous Fe(II) and hydrous ferric oxide. Environ. Sci. Technol. 45(5), 1847-
939 1852.
940 Zhu, X.K. et al., 2002. Mass fractionation processes of transition metal isotopes. Earth Planet.
941 Sci. Lett. 200(1-2), 47-62.